Modeling the summertime evolution of sea-ice melt ponds

M. Lüthje

Ørsted-DTU, Electromagnetic Systems, Technical University of Denmark, Lyngby, Denmark

D. L. Feltham[1] and P. D. Taylor

Centre for Polar Observation and Modelling, Department of Space and Climate Physics, University College London, London, UK

M. G. Worster

Institute of Theoretical Geophysics, Department of Applied Mathematics and Theoretical Physics, University of Cambridge, Cambridge, UK

[1] We present a mathematical model describing the summer melting of sea ice. We simulate the evolution of melt ponds and determine area coverage and total surface ablation. The model predictions are tested for sensitivity to the melt rate of unponded ice, enhanced melt rate beneath the melt ponds, vertical seepage, and horizontal permeability. The model is initialized with surface topographies derived from laser altimetry corresponding to first-year sea ice and multiyear sea ice. We predict that there are large differences in the depth of melt ponds and the area of coverage between the two types of ice. We also find that the vertical seepage rate and the melt rate of unponded ice are important in determining the total surface ablation and area covered by melt ponds.

Citation: Lüthje, M., D. L. Feltham, P. D. Taylor, and M. G. Worster (2006), Modeling the summertime evolution of sea-ice melt ponds, *J. Geophys. Res.*, *111*, C02001, doi:10.1029/2004JC002818.

1. Introduction

[2] During winter, Arctic sea ice is covered by snow creating a highly uniform reflective layer with an albedo of 0.8–0.9 [*Langleben*, 1968; *Grenfell and Perovich*, 1984; *Perovich et al.*, 2002a]. During spring and summer, the Arctic undergoes a dramatic change: There is an increase in ambient temperature, cloud cover, precipitation, and solar radiation [*Derksen et al.*, 1996; *Papakyriakou*, 1999]. The snow cover melts more or less completely, exposing sea ice to solar radiation, and the sea ice melts at its upper surface. Some of the meltwater runs off the edges of the ice floes and entrains into the ocean mixed layer [*Ebert and Curry*, 1993], and some drains vertically through the sea ice and may form under-ice ponds of relatively fresh, and therefore buoyant, water [*Notz et al.*, 2003]. Meltwater on the sea-ice surface forms ponds with depths of several centimeters to more than a meter deep [*Eicken*, 1994].

[3] *Laxon et al.* [2003] used data from radar altimeters carried on the ERS-1 and ERS-2 satellites to find a significant correlation between the length of a melt season and the departure from the interannual mean of winter ice thickness in the subsequent winter. This could indicate that the physics of melt-pond formation and evolution play an important role in determining the amount of ice melted. Certainly, melt ponds are an important factor determining the albedo of the summer sea ice cover, because they have a lower albedo than the surrounding ice. The albedo of a melt pond ranges between 0.1 and 0.5 [*Hanesiak et al.*, 2001; *Grenfell and Maykut*, 1977] whereas the albedo of white ice ranges between 0.39 and 0.84 [*Fetterer and Untersteiner*, 1998; *Makshtas and Podgorny*, 1996]. The large-scale, i.e., area-averaged, albedo of ponded ice can be as low as 0.4 compared to 0.65 for non-ponded, bare white ice [*Perovich et al.*, 2002a]. It has been hypothesized that an increase in surface melt of sea ice will lead to greater melt-pond coverage, decreasing the area-averaged albedo, which will in turn lead to more absorption of radiation and further melting. Melt ponds therefore enhance the albedo feedback mechanism [*Morassutti*, 1992; *Perovich and Tucker*, 1997]. The albedo of the ice cover is parameterized in the sea-ice component of General Circulation Models (GCMs) such as the latest Los Alamos CICE model version 3.1 (http://climate.lanl.gov/Models/CICE/) in a manner that does not explicitly treat melt ponds. See *Perovich et al.* [2002a] for a discussion of GCM sea ice albedo schemes.

[4] The area of melt-pond cover has been most extensively studied by use of aircraft, balloons and, to a lesser extent, satellites. These studies indicate a summer area of coverage of between 5 and 80% depending on such factors as surface roughness, snow cover, and time elapsed since the beginning of the melt season [*Barber and Yackel*, 1999; *Derksen et al.*, 1997; *Fetterer and Untersteiner*, 1998; *Perovich and Tucker*, 1997; *Tschudi et al.*, 2001]. A typical value of the area of coverage of melt ponds for shorefast old ice and first-year ice in the Northeast Water Polynya east of Greenland is 14% and 48%, respectively [*El Naggar et al.*,

---

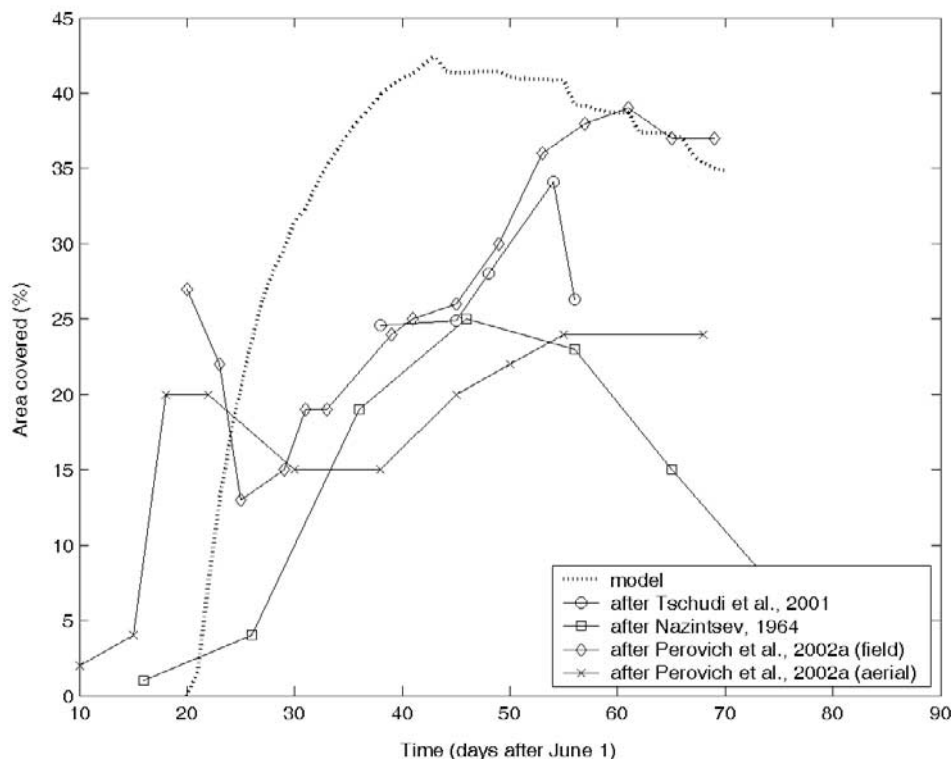[1] Also at British Antarctic Survey, Cambridge, UK.

Figure 1. Area of melt-pond cover from field studies and simulated by our model. The model used an initial multiyear sea ice topography, seepage rate $s = 0.8$ cm/day, unponded ice melt rate $m_i = 1.2$ cm/day, maximum melt pond enhanced melt rate $m_p = 2$ cm/day, and horizontal permeability $\Pi_h = 3 \times 10^{-9}$ m^2.

1998]. From ice-camp fieldwork, the area coverage of melt ponds has been reported within the same range [*Perovich et al.*, 2003]. Several different studies have reported evolution of the area of coverage over the summer melt season [*Nazintsev*, 1964; *Perovich et al.*, 2002b; *Tschudi et al.*, 2001] (Figure 1).

[5] It has been suggested that the spatial distribution of melt ponds depends on the topography of the ice and snow [*Barber and Yackel*, 1999; *Derksen et al.*, 1997]. First-year sea ice tends to be smoother than multiyear ice and melt ponds on first-year ice are normally less deep [*Morassutti and LeDrew*, 1996] but cover a greater area [*Hanesiak et al.*, 2001]. The distribution of melt ponds on first-year ice is strongly linked to the winter distribution of snow so that areas with little or no snow during winter are preferred places for the ponds to form [*Derksen et al.*, 1997; *Hanesiak et al.*, 2001]. On rougher sea ice, such as multiyear ice, melt ponds form in depressions [*Fetterer and Untersteiner*, 1998] and tend to be smaller, deeper, and more numerous [*Yackel et al.*, 2000].

[6] Early thermodynamic models of sea ice characterized summer albedo with a lower value than that used for winter months [see, e.g., *Maykut and Untersteiner*, 1971]. Not until 1993 was a sea-ice model developed that included a parameterization of the thermal and radiative effect of melt ponds [*Ebert and Curry*, 1993]. Recently, a more sophisticated thermodynamic-radiative model that explicitly treats the melt pond as an extra phase was developed and forced with real climate data. This model has succeeded in modeling the depth evolution of melt

ponds [*Taylor and Feltham*, 2004]. All of these models, however, have been formulated in one vertical dimension and give limited insight into the horizontal evolution of the sea-ice cover.

[7] In this paper we present a model that describes both the vertical and horizontal evolution of the sea-ice cover during summer. The purpose of this model is to investigate which factors, such as surface topography, melt rate, vertical seepage rate, and horizontal permeability, are important in controlling the evolution in the area of coverage of melt ponds and the total summer surface ablation.

[8] The paper is divided as follows: the next section describes the model developed to simulate the summer evolution of sea ice; in section 3, some of the model assumptions are discussed; in section 4, the area evolution, pond depth and total surface ablation among other results are presented; in section 5, these results are discussed; and, finally, in section 6, we summarize our main conclusions.

2. Mathematical Model of Melt Pond Evolution

[9] We develop a two-dimensional cellular automaton in which each cell represents a region of the ice surface with a certain depth of meltwater. Figure 2 illustrates a volume element containing part of the surface of the sea-ice cover. The volume element is in the shape of a square prism with horizontal edges of width δx and δy, which are parallel to the axes of a Cartesian coordinate system fixed in space. The upper surface of the sea ice is given by $z = H_t$ with respect to a fixed plane $z = 0$ and the depth of the layer of meltwater
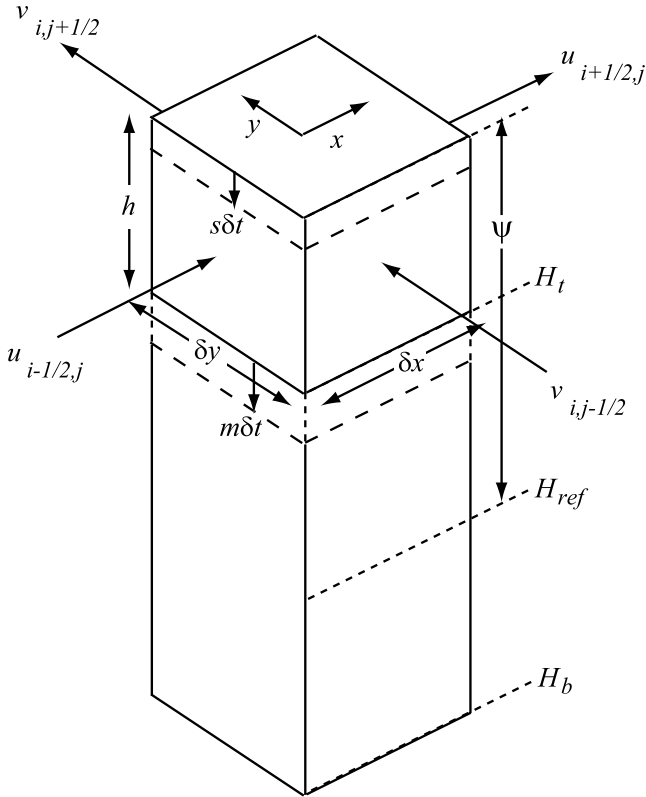
Figure 2. Volume element containing part of the sea-ice surface (the upper box) and sea ice column below. Here δx and δy are the width and breadth, and h is the height of, the surface volume element; H_t is the upper surface of the sea ice and H_b is the lower surface (bottom) of the sea ice; H_{ref} is a reference level and Ψ is the surface topography given by $\Psi \equiv H_t + h - H_{ref}$; $\mathbf{u} = (u, v)$ is the horizontal flux of meltwater per unit cross-sectional area into and out of the volume element; s is the vertical seepage rate and m is the melt rate. The suffixes i, j refer to the horizontal location of the volume element with respect to the coordinate system.

on top of the sea ice is denoted by h. The surface topography is given by $\Psi \equiv H_t + h - H_{ref}$, where H_{ref} is some reference level. The depth of the sea ice is given by $H = H_t - H_b$, where $z = H_b$ is the lower surface (bottom) of the sea ice. The suffixes i, j refer to the horizontal location of the volume element with respect to the coordinate system. The dashed lines illustrate how the

surface of the melt pond will lower after a time interval δt owing to vertical seepage s and the upper surface of the sea ice will lower owing to melting m. The horizontal fluxes of meltwater into or out of the volume element per unit cross-sectional area are denoted by u and v along the x and y axes, respectively, and are evaluated on the horizontal faces of the volume element.

[10] Referring to Figure 2, we see that in a small time step δt, conservation of the mass of the meltwater in the volume element can be written as

$$\delta y \delta x h_{i,j}^{t+\delta t} = \delta y \delta x h_{i,j}^{t} - s \delta t \delta x \delta y + \frac{\rho_{ice}}{\rho_{water}} m \delta t \delta x \delta y$$
$$+ \delta t h_{i,j}^{t} \left(u_{i-\frac{1}{2},j} \delta y - u_{i+\frac{1}{2},j} \delta y + v_{i,j-\frac{1}{2}} \delta x - v_{i,j+\frac{1}{2}} \delta x \right),$$

which, upon dividing by $\delta x \delta y \delta t$ and taking the limit as $\delta t \to 0$, $\delta x \to 0$, $\delta y \to 0$, yields

$$\frac{\partial h}{\partial t} = \text{He}(h) \left(-s + \frac{\rho_{ice} \cdot m}{\rho_{water}} - \nabla \cdot (h\mathbf{u}) \right), \quad (1)$$

where $\nabla \equiv (\partial/\partial x, \partial/\partial y)$ is the horizontal gradient, $\mathbf{u} = (u, v)$ is the horizontal flux vector of meltwater per unit cross-sectional area, and $\text{He}(h)$ is the Heaviside function, where $\text{He}(h) = 1$, $h \geq 0$, $\text{He}(h) = 0$, $h < 0$. The Heaviside function prevents the meltwater depth h becoming negative; if $h = 0$ in a given time step, h may increase in subsequent time steps if the water produced from melting exceeds that lost from seepage and horizontal drainage but cannot decrease. We take the water density to be $\rho_{water} = 1000$ kg/m^3 and the ice density to be $\rho_{ice} = 900$ kg/m^3. Ice densities of 800 kg/m^3, 850 kg/m^3 and 950 kg/m^3 were, however, also tested.

[11] The calculation of meltwater flow through sea ice, which is a reactive porous medium, is complex and challenging and beyond the scope of this paper. *Eicken et al.* [2002, 2004] address this topic. Instead, we introduce a relatively crude approximation of meltwater flow and examine the model sensitivity to the parameters in this approximation. The permeability of sea ice is a tensor that is typically orthotropic [*Freitag*, 1999; *Feltham et al.*, 2002]. The permeability to flows parallel to the columns (dendrites), normally aligned vertically, is much greater than the permeability to flows across the columns. The implication of this is that for equal pressure gradients, meltwater flows more rapidly vertically through the sea ice than horizontally. We treat the vertical seepage rate s as a

Table 1. Summary of Results for Model Runs With First-Year Ice (FYI) and Multiyear Ice (MYI) Topographies[a]

Ice Type	Mean Ice Thickness, m	Standard Deviation	Maximum Ice Thickness, m	Minimum Ice Thickness, m	Maximum Pond Area Covered	Mean Pond Area Covered	Maximum Mean Pond Depth, m	Maximum Pond Depth, m	Mean Surface Ablation, m
FYI1	0.90	0.12	1.26	0.40	0.83	0.41	0.18	0.51	0.76
FYI2	0.93	0.12	1.39	0.5	0.89	0.46	0.19	0.56	0.79
FYI3	0.93	0.31	2.59	0.32	0.7	0.35	0.15	0.43	0.70
FYI-mean	0.92	0.18	1.75	0.41	0.81	0.41	0.17	0.50	0.75
MYI1	4.12	1.65	13.2	0.2	0.42	0.34	0.65	1.20	0.92
MYI2	4.31	1.52	12.7	0.9	0.55	0.41	0.62	1.15	0.99
MYI3	3.65	1.65	20.8	0.5	0.47	0.34	0.52	1.20	0.92
MYI4	2.61	1.18	14.2	0	0.36	0.27	0.50	1.14	0.82
MYI-mean	3.67	1.50	15.23	0.40	0.45	0.34	0.57	1.17	0.91

[a]The parameter values used were $\Pi_h = 3 \times 10^{-9}$ m^2, $s = 0.8$ cm/day, $m_i = 1.2$ cm/day, and $m_p = 2$ cm/day. The mean pond area covered is for the entire period for multiyear ice but only for the first 35 days for first-year ice since a large fraction of the ice after that date had melted completely.
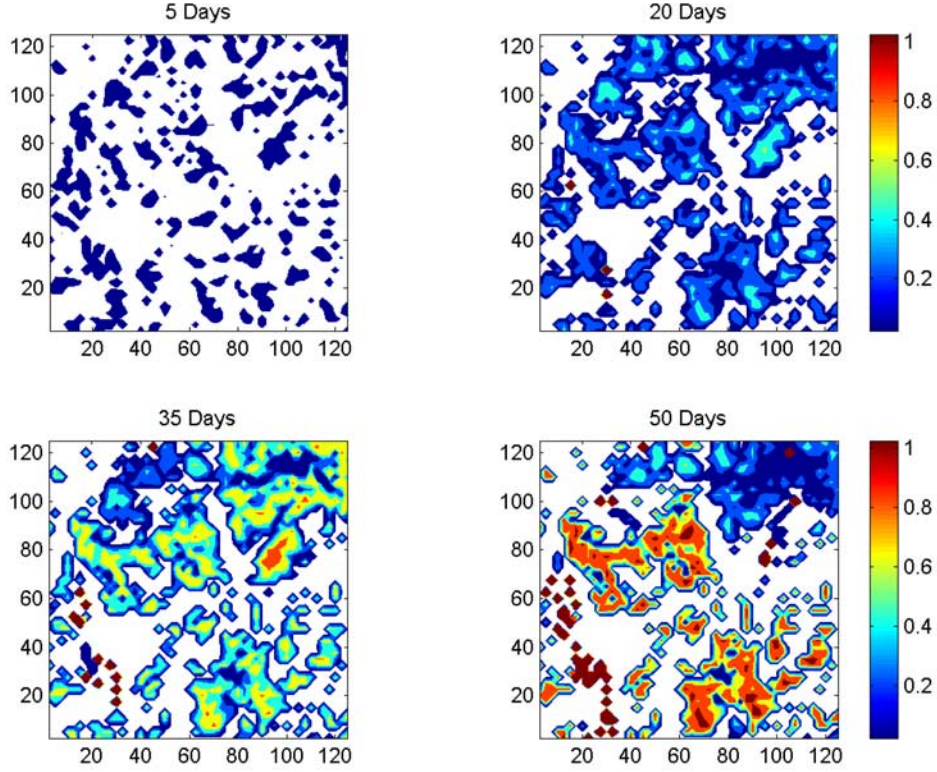
Figure 3a. Model output showing the evolution of melt pond depth and area on multiyear ice after 5, 20, 35, and 50 days. The axes are labeled in meters. The dark red areas show where the sea ice has melted through completely. The average melt pond area after 5 days is 17 m², after 20 days it is 69 m², after 35 days it is 67 m², and after 50 days it is 51 m². The model used an initial multiyear sea ice topography, seepage rate $s = 0.8$ cm/day, unponded ice melt rate $m_i = 1.2$ cm/day, maximum melt pond enhanced melt rate $m_p = 2$ cm/day, and horizontal permeability $\Pi_h = 3 \times 10^{-9}$ m². The model domain size was 125 m by 125 m.

constant, and examine the predictions of the model to variations in this parameter.

[12] As vertical seepage occurs more rapidly than horizontal redistribution through the surface layer, in each time step of the numerical calculations, we apply the horizontal flux of meltwater into, or out of, a grid cell only if there is meltwater left after vertical seepage has taken place. The horizontal fluxes of meltwater are driven by horizontal pressure gradients caused by variations in the height of the melt surface. The top layer of the sea ice becomes crusty and porous during summer [Hanesiak et al., 2001] and, in order for the meltwater to move horizontally to an adjacent location of lower gravitational potential, it must pass through barriers of porous sea ice. We describe the flow of meltwater through this porous sea ice using Darcy's Law so that the horizontal mass flux per unit cross-sectional area is

$$\mathbf{u} = -\frac{g\rho_{water}}{\mu} \Pi_h \nabla \Psi, \qquad (2)$$

where g is gravitational acceleration, μ is the dynamic viscosity, equal to 1.79×10^{-3} kg/(m s^{-1}) [Kundu, 1990], and Π_h is the horizontal permeability of sea ice (with units of length squared). As the porous barriers through which

the meltwater must flow are typically more narrow than the grid resolution used for numerical calculations presented later, the numerically calculated derivatives will be too small and the flux given by equation (2) will be an underestimate. In order to account for this, we artificially enhance the value of the permeability by a constant factor, which is equivalent to increasing the magnitude of the derivatives. We explore the model sensitivity to variations in the horizontal permeability.

[13] If the amount of horizontal drainage from one grid cell to its neighbors, predicted by equation (2), is greater than the amount of water available, the total amount of horizontal drainage is set equal to the water available after melting and seepage, and the horizontal transports to the adjacent cells are weighted according to the topography gradients across each pair of cells. If meltwater is transported by horizontal drainage into a cell where the ice thickness is zero, the meltwater is assumed to enter the ocean and is lost.

[14] Combining equations (1) and (2) allows us to write conservation of mass of the meltwater as

$$\frac{\partial h}{\partial t} = \mathrm{He}(h)\left(-s + \frac{\rho_{ice} \cdot m}{\rho_{water}} - \frac{g\rho_{water}}{\mu}\Pi_h \nabla \cdot (h\nabla\Psi)\right). \quad (3)$$
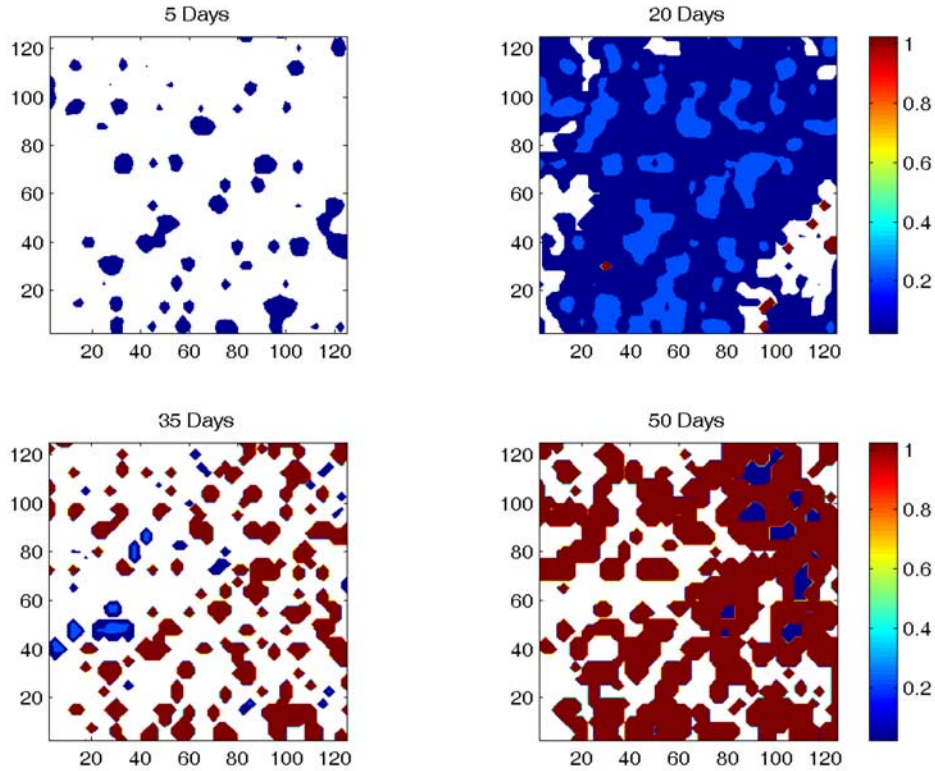
Figure 3b. Model output shows the evolution of melt pond depth and area on first-year sea ice after 5, 20, 35, and 50 days. The axes are labeled in meters. The dark red areas show where the sea ice has melted through completely. The average melt pond area after five days is 27 m^2, after 20 days it is 1202 m^2, and after 35 days it is 13 m^2. The model used an initial first-year sea ice topography, seepage rate s = 0.8 cm/day, unponded ice melt rate m_i = 1.2 cm/day, maximum melt pond enhanced melt rate m_p = 2 cm/day, and horizontal permeability $\Pi_h = 3 \times 10^{-9}$ m^2. The model domain size was 125 m by 125 m.

Equation (3) states that the rate of change of pond depth (first term) is due to the loss from seepage (second term), the gain from melting at the pond base (third term), and mass gained from or lost to the surrounding area (fourth term).

[15] Melt ponds have a lower albedo than the surrounding ice and therefore more radiation is transmitted to the sea ice beneath the pond. This extra radiation, combined with an enhanced energy transport rate due to convection in the ponds [Taylor and Feltham, 2004], leads to an enhanced melt rate beneath them. The enhanced melt rate is a function of the melt pond depth since deeper ponds tend to have a lower albedo [Morassutti and LeDrew, 1996; Hanesiak et al., 2001]. In this model, we prescribe a constant summer melt rate for unponded ice, m_i, and the total melt rate is given by

$$m = Em_i, \qquad (4)$$

where

$$E = \left(1 + \frac{m_p}{m_i}\frac{h}{h_{\max}}\right) \quad 0 \leq h \leq h_{\max}$$
$$E = 1 + \frac{m_p}{m_i} \quad h > h_{\max} \qquad (5)$$

is the enhancement factor due to the presence of melt ponds, m_p is a constant parameter, and $h_{\max}$ is the pond depth beyond which melting is no longer enhanced (see discussion in the next section). The melt rates are in meters of ice and not water equivalent.

[16] The equation for the evolution of sea-ice surface height H_t, and hence topography, is given by

$$\frac{\partial H_t}{\partial t} = \frac{\partial \Psi}{\partial t} - \frac{\partial h}{\partial t} = \text{He}(H)(-m), \qquad (6)$$

which states that the ice surface H_t lowers owing to melting at the pond base. When $H = 0$, the sea ice has melted through completely, and we no longer track the topography.

[17] To solve the system (3), (4) and (6), the model equations were discretized using finite differences and the resulting algebraic equations solved numerically. A horizontal, rectangular domain divided by a grid into square elements with edge length Δx was used, with vertices indexed by $i = 1, \ldots, M$ and $j = 1, \ldots, N$ so that $L_x = M \cdot \Delta x$ and $L_y = M \cdot \Delta x$ define the edge lengths of the computational domain. The time step Δt is indexed by $t = 1, \ldots, T$. The maximum time step used was 60 s.

[18] An initial topography and ice thickness distribution was imposed, assuming no snow cover present. The initial surface topography $\Psi_{i,j}^0$ comes from altimetry field measurements and is the freeboard. The initial sea-ice thick-
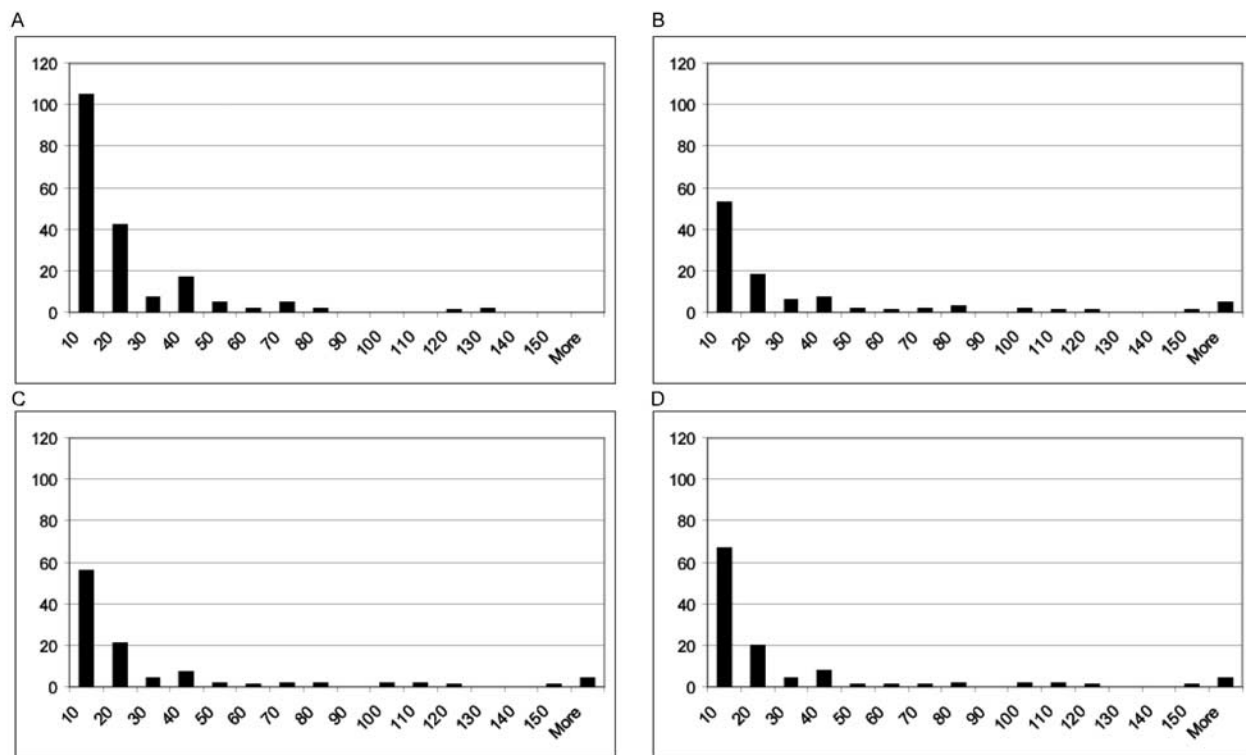
Figure 4a. The melt pond area distribution after (graph A) 5, (graph B) 20, (graph C) 35, and (graph D) 50 days for a multiyear sea ice topography. The scale on the abscissa axis is area in meters squared, and on the ordinate axis it is the number of ponds with a given area. The model used an initial multiyear sea ice topography, seepage rate $s = 0.8$ cm/day, unponded ice melt rate $m_i = 1.2$ cm/day, maximum melt pond enhanced melt rate $m_p = 2$ cm/day, and horizontal permeability $\Pi_h = 3 \times 10^{-9}$ m^2.

ness $H_{i,j}^0$ was calculated from this freeboard, assuming hydrostatic equilibrium, according to

$$H_{i,j}^0 = \frac{\Psi_{i,j}^0}{1 - (\rho_{ice}/\rho_{water})}, \qquad (7)$$

which, while clearly an approximation, nonetheless yields reasonable ice thicknesses, when $\rho_{ice} = 900$ kg/m^3.

[19] As we wish to model a representative region of the sea-ice cover, periodic boundary conditions were used; that is, water that is transported horizontally out of one edge of the domain enters the domain again from the opposite edge. This means that edge effects, and in particular the run-off of meltwater from floe edges, are not modeled.

[20] The model was run for a prescribed number of days to simulate the melt season. Since freezing processes are not modeled, the disappearance of the ponds through refreezing cannot be simulated realistically.

3. Discussion of Model Assumptions

[21] The model we have introduced is a simple representation of the physics of summer melt and, as such, it naturally has some limitations. Seven initial sea-ice topographies were used, three corresponding to first-year ice and four corresponding to multiyear ice, processed from raw data collected as part of a laser scanning campaign in the

Fram Strait, 2003 (R. Forsberg, personal communication, 2004). The first-year ice was identified as distinct from the multiyear ice on the basis of different ENVISAT ASAR mean backscatter and texture characteristics, and different mean thicknesses; the mean ice thickness was 0.92 m for first-year ice and 3.67 m for multiyear ice. Height data of sea ice from laser scanning cannot differentiate between snow and ice. The data measured are in meters above the geoid and have been converted into ice thickness by assuming that the geoid is constant within a small area and that the lowest values in the data set correspond to open leads (sea level). The sampling method is explained in detail in *Hvidegaard and Forsberg* [2002]. The estimated accuracy of the measured ice freeboard is 13 cm [*Hvidegaard and Forsberg*, 2002]. The variations in the surface topography for first-year ice are on the limit of the laser scanner's vertical resolution. It is therefore possible that some of the surface topography is created by noise in the measurements and the ice is actually smoother. Equally, there could be small-scale roughness not resolved by the laser scanner. Our model does not explicitly treat the snow cover and, as the topography we use does not distinguish between snow and ice, this is equivalent to assuming the same melt rate for the snow and ice.

[22] The total surface ablation at the end of the melt season depends directly upon the length of the melt season in our model as we use the same melt rate throughout. The use of a constant melt rate is a fair approximation to the melt
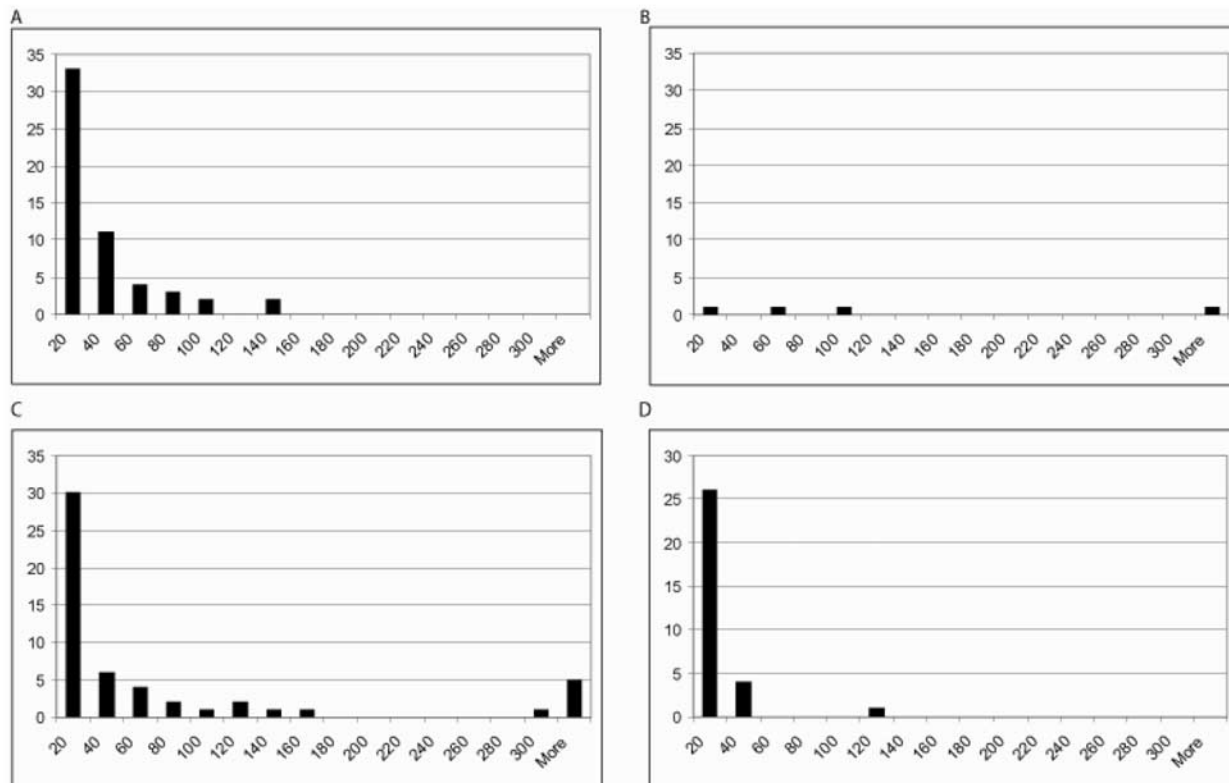
Figure 4b. The melt pond area distribution after (graph A) 5, (graph B) 10, (graph C) 20, and (graph D) 30 days for a first-year sea ice topography. After 5 days the area distribution consists only of many small melt ponds, the melt ponds then grow together forming fewer but larger ponds. After 20 days some of the melt ponds have melted through the sea ice draining the surrounding area leaving mostly small ponds behind. After 30 days, basically all the melt ponds have disappeared. The scale on the abscissa axis is area in meters squared, and on the ordinate axis it is the number of ponds with a given area. The model used an initial first-year sea ice topography, seepage rate $s = 0.8$ cm/day, unponded ice melt rate $m_i = 1.2$ cm/day, maximum melt pond enhanced melt rate $m_p = 2$ cm/day, and horizontal permeability $\Pi_h = 3 \times 10^{-9}$ m^2.

rate calculated in the numerical simulations of *Taylor and Feltham* [2004], and the dependence of total surface ablation on the length of melt season is also in accordance with analysis of satellite-derived thickness data [*Laxon et al.*, 2003]. *Smith* [1998] used observations from passive microwave radiometers to estimate the length of the melt season during 1994 to 2001 and found a mean duration of 65 days. We use a melt season length of 50 days, which is comparable to other model studies [*Ebert and Curry*, 1993; *Ebert et al.*, 1995; *Maykut and Untersteiner*, 1971; *Taylor and Feltham*, 2004; *Untersteiner*, 1961], and is reasonable owing to the simplicity of our melting scheme and because we do not treat refreezing.

[23] Our model uses three input parameters to calculate the melt rate, m_i, m_p, and h_{max}, which are held constant throughout the melt season. During the SHEBA (Surface Heat Budget of the Arctic Ocean) campaign, the total surface ablation of ponded ice was measured and found to have an average of 0.75 m with a minimum of 0.4 m and a maximum of 1.09 m [*Perovich et al.*, 1999]. In situ measurements from the Beaufort Sea (1997) suggest melt rates of unponded ice, m_i, of 0.8–1.8 cm/day [*Eicken et*

al., 2001]. Many different values of the melt rate of unponded ice have been tested, ranging from 0.20 cm/day to 3.5 cm/day. For a melt season length of 50 days, these melt rates for unponded ice would imply a total surface ablation for unponded ice of between 0.10 m to 1.75 m. Model results suggest values of m_i of 0.6 cm/day to 1.2 cm/day are probably most realistic [*Taylor and Feltham*, 2004], although these have not been validated from field measurements. The wider range of melt rates were used to examine model sensitivity to m_i.

[24] In an extensive study of four sea ice sites in the Canadian Arctic Archipelago, over 500 in situ measurements of melt ponds were carried out over a period of 1 month [*Morassutti*, 1995; *Morassutti and LeDrew*, 1996]. Comparing depth and albedo measurements showed that albedo decreases with depth up to a critical depth beyond which the albedo is constant. This happened at different depths depending on the cloud conditions and, for broadband albedo, this critical depth was measured to be between 0.4 m and 0.26 m. A similar result was found from measurements of first-year sea ice in the Wellington Channel [*Hanesiak et al.*, 2001]; that is, the deeper the
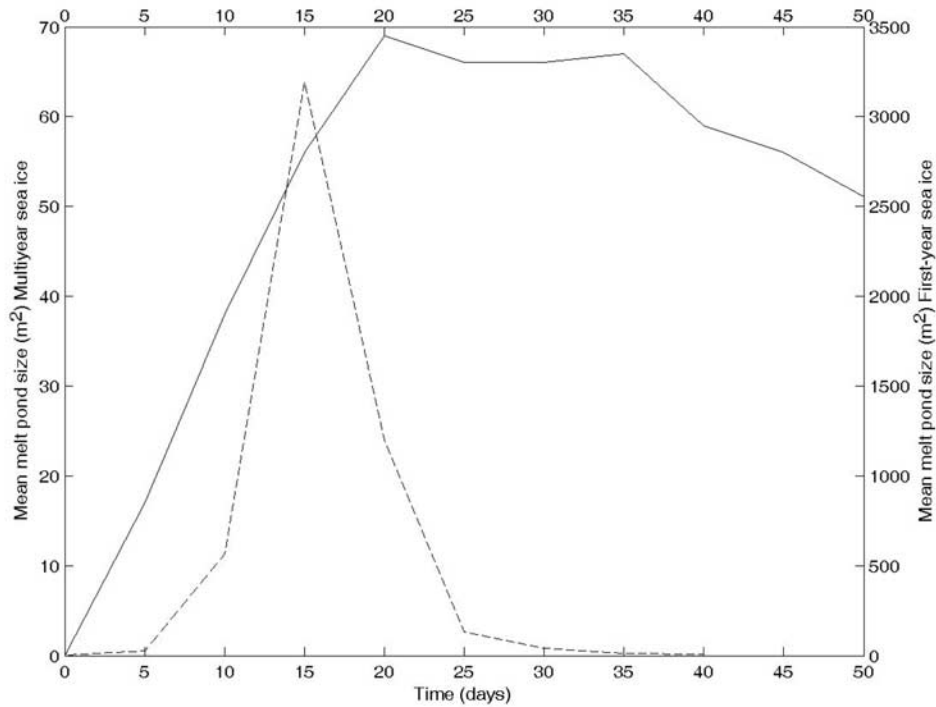
Figure 5. Average melt pond area as a function of time. The solid line shows results for a multiyear sea ice topography (scale on left-hand side) and the dashed line for a first-year sea ice topography (scale on right-hand side). The model used a seepage rate $s = 0.8$ cm/day, unponded ice melt rate $m_i = 1.2$ cm/day, maximum melt pond enhanced melt rate $m_p = 2$ cm/day, and horizontal permeability $\Pi_h = 3 \times 10^{-9}$ m^2.
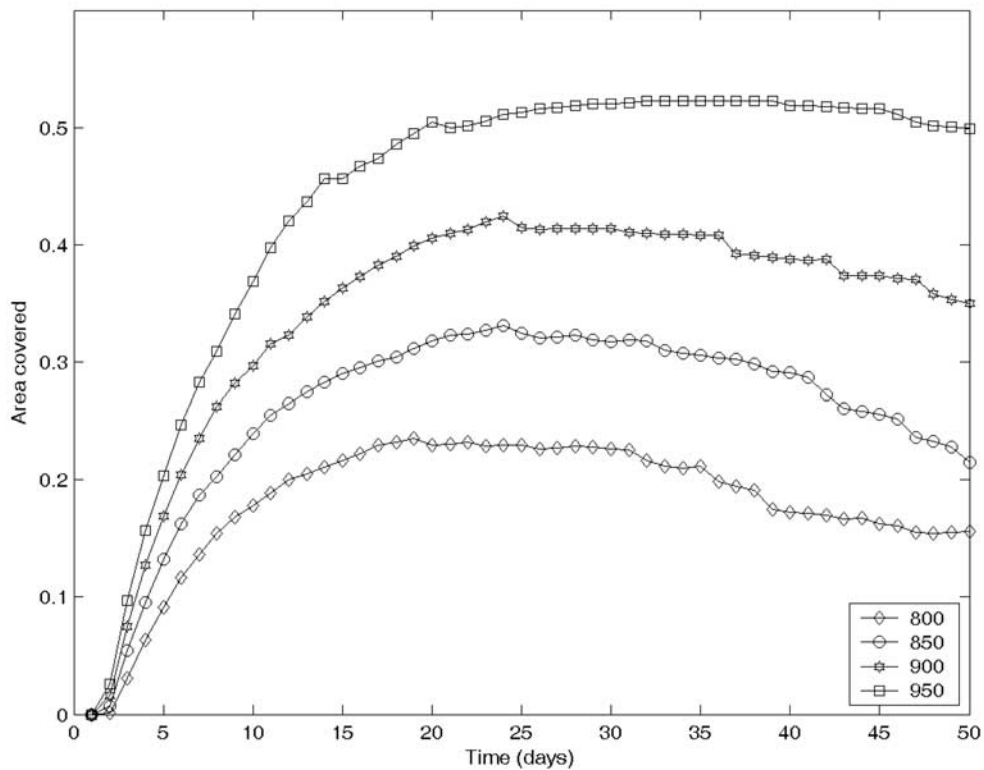

Figure 6. Area covered by melt ponds on multiyear sea ice for varying densities. The legend shows the value of the density in kg/m^3. The model used a seepage rate $s = 0.8$ cm/day, unponded ice melt rate $m_i = 1.2$ cm/day, maximum melt pond enhanced melt rate $m_p = 2$ cm/day, and horizontal permeability $\Pi_h = 3 \times 10^{-9}$ m^2.
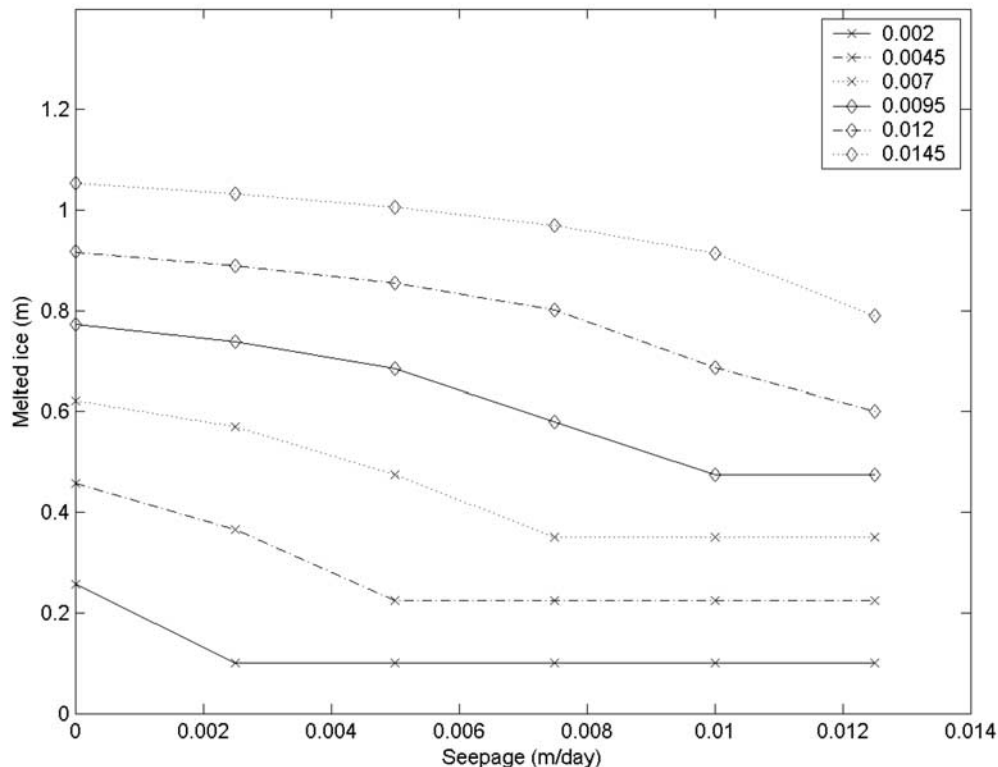
Figure 7a. Total amount of surface ablation is shown for different seepage rates s and unponded melt rates m_i for multiyear sea ice. The legend shows the melt rate for unponded ice in m/day. The model was initialized with a multiyear sea ice topography, a horizontal permeability $\Pi_h = 3 \times 10^{-9}$ m^2, and a maximum melt pond enhanced melt rate $m_p = 1$ cm/day.

pond, the lower the albedo (the deepest pond reported was 0.23 m). However, beyond a depth of 0.1 m, the decrease in measured albedo was tiny. From these measurements, it was decided to set $h_{max} = 0.1$ m.

[25] Enhanced melt rates beneath melt ponds relative to surrounding unponded ice of up to 2–3 times have been quoted by *Fetterer and Untersteiner* [1998]. Different values of m_p were tested to model this enhanced melt rate. We have performed two sets of calculations using values of m_p equal to 1 cm/day and 2 cm/day. Higher values of m_p have also been tested to examine the sensitivity of total surface ablation and the area of melt-pond cover to this parameter. Since horizontal transport of meltwater occurs by flowing across and through the top, very porous layer of sea ice, a thin layer of water must be allowed to be present all over the ice surface and this should not be treated as a melt pond. To clearly differentiate melt ponds from the surrounding ice, the enhanced melt rate was used only for meltwater depths greater than 0.025 m.

[26] The treatment of meltwater flow through the summer sea ice cover is probably the weakest area of the model physics and is most poorly constrained. The meltwater flow is calculated using the parameters s and Π_h. In our model, a greater seepage rate than melt rate for unponded ice, $s > m$, would drain all the meltwater and no melt ponds would form. A wide range of seepage rates were tested spanning from $s = 0$ to 1.25 cm/day.

[27] The meltwater that is not drained vertically is allowed to flow laterally. As discussed in the previous section, the horizontal meltwater transport is driven by horizontal variations in topography and occurs by flow through porous barriers of sea ice. We use Darcy's law to describe this lateral flow but, as the porous barriers through which the meltwater must flow are typically narrower than the grid cell resolution, we artificially enhance the horizontal permeability of the sea ice. We tested 100 different values of horizontal permeability, ranging from $\Pi_h = 10^{-11}$ m^2 to 10^{-6} m^2 and adopted a standard value of 3×10^{-9} m^2 as this gave reasonable pond area fractions. This value of the horizontal permeability is slightly higher than the permeability measured during SHEBA [*Eicken et al.*, 2002].

4. Results

[28] Model calculations showed little sensitivity of the total pond coverage and surface ablation to grid sizes less than 2.5 m and thus $\Delta x = 2.5$ m was used for all the calculations presented in this paper. All the multiyear sea ice and the first-year sea ice domains were of area 125 m × 125 m. A standard set of parameters was chosen to be $s = 0.8$ cm/day, $m_i = 1.2$ cm/day, $m_p = 2$ cm/day, $h_{max} = 0.1$ m, and $\Pi_h = 3 \times 10^{-9}$ m^2. With these parameter values, the model was ran using seven different initial sea ice topographies. Table 1 summarizes the mean ice thickness, the standard deviation of the ice thickness, the maximum ice thickness, and the minimum ice thickness of the initial topographies, and the maximum area
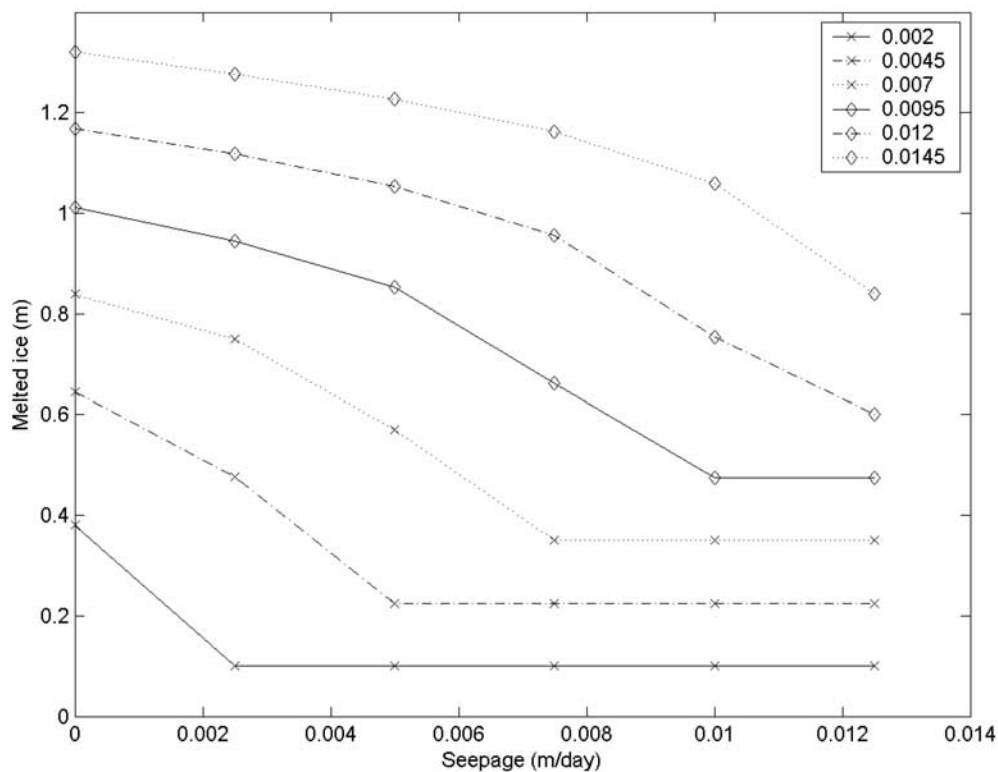
Figure 7b. Total amount of surface ablation is shown for different seepage rates s and unponded melt rates m_i for multiyear sea ice. The legend shows the melt rate for unponded ice in m/day. The model was initialized with a multiyear sea ice topography, a horizontal permeability $\Pi_h = 3 \times 10^{-9}$ m^2, and a maximum melt pond enhanced melt rate $m_p = 2$ cm/day.

covered by melt ponds, the mean area covered by melt ponds, the maximum mean pond depth, the maximum pond depth, and the mean surface ablation calculated using our model.

[29] The mean thickness of the initial first-year ice topographies was quite thin (0.92 m) and showed little spatial variation compared to the initial topographies of thicker multiyear ice (with mean thickness of 3.67 m). For comparison, the multiyear ice investigated during SHEBA had a mean thickness of only about 2 m [*Eicken et al.*, 2001; *McPhee et al.*, 1998].

[30] The maximum area covered by melt ponds calculated by our model varied from 0.7 to 0.89 for first-year ice and between 0.36 and 0.55 for multiyear ice. Almost complete melt pond coverage has been observed on first year, shore-fast ice [*Holt and Digby*, 1985]. From measurement at Barrow in 2001 the maximum areal pond fraction for first-year ice was 0.6 [*Eicken et al.*, 2004], whereas at SHEBA the melt ponds fractional coverage was up to 0.46 and 0.21 for level and rough multiyear ice respectively [*Eicken et al.*, 2004]. Melt ponds are often found to cover around twice the area on first-year ice than multiyear ice [*El Naggar et al.*, 1998; *Hanesiak et al.*, 2001].

[31] The calculated mean area covered by melt ponds was found to be 0.34 for multiyear ice, which can be compared with measurements during SHEBA of 0.32 and 0.13 for level and rough multiyear ice, respectively [*Eicken et al.*,

2004]. This mean area of coverage is somewhat higher than the observations by *El Naggar et al.* [1998] of 0.20. The calculated mean area covered by melt ponds on first-year ice was 0.41. Although this is somewhat higher than the mean value of 0.19 measured for first year ice by *Eicken et al.* [2004], it is comparable with the value of 0.34 found by *El Naggar et al.* [1998].

[32] The calculated area covered by melt ponds peaked after 21 to 29 days for multiyear ice and after 15 to 18 days for first-year ice. The time to reach peak coverage for first-year ice corresponds well with the observations of *Hanesiak et al.* [2001], who found that on Julian day 175 no melt ponds were present but by day 193 ponds covered 75% of the surface. It should be noted, however, that since our model does not model snow explicitly, this comparison should be treated with some caution.

[33] The calculated maximum mean pond depth was found to be 17 cm for first-year ice and 57 cm for multiyear ice which is in accordance with the observation that melt ponds on multiyear ice are typically deeper than melt ponds on first-year ice [*Yackel et al.*, 2000]. Although *Morassutti and LeDrew* [1996] reported a mean melt pond depth of 13 cm on first-year ice and 27 cm on multiyear ice, this was the mean over their observational period and is not the maximum mean melt pond depth. *Yackel et al.* [2000] reported a maximum melt pond depth of about 40 cm and 65 cm for first-year ice and multiyear ice, respectively.
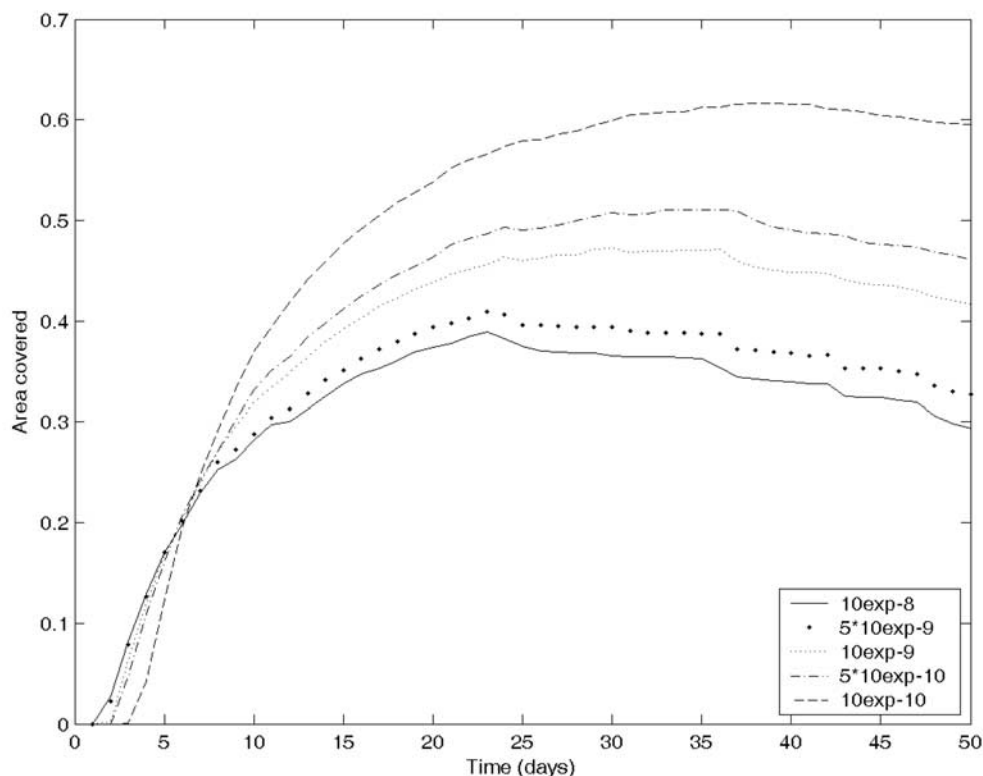
Figure 8a. Area covered by melt ponds on multiyear sea ice for varying horizontal permeabilities Π_h. The legend shows the value of the horizontal permeability in m^2. The model used an initial multiyear sea ice topography, seepage rate $s = 0.8$ cm/day, unponded ice melt rate $m_i = 1.2$ cm/day, and maximum melt pond enhanced melt rate $m_p = 2$ cm/day.

[34] The calculated mean surface ablation was 75 cm for first year ice and 91 cm for multiyear ice. The sensitivity of the model calculations to the choice of model parameters and a further discussion of their relation to field observations are given below and in section 5.

[35] One first-year ice topography (FYI 1) and one multiyear ice topography (MYI 1) topography were chosen to be used for this investigation. Using the standard set of parameter values, the model produced the melt pond area distribution and depths shown in Figure 3a for multiyear sea ice and in Figure 3b for first-year sea ice. The dark red colored areas in the figures are where the ice has melted through completely. In both cases, many small melt ponds are produced initially and these then grow together until the total area covered by melt ponds peaks (see Figures 4a and 4b). As the melt ponds deepen, some melt through the thinner ice completely, and the total area covered by melt ponds diminishes. The peak in melt pond area coverage for first-year ice is about 80%, which occurs after approximately 2 weeks. Since the first-year ice is relatively thin, it almost completely melts away. The maximum melt pond area coverage for multiyear ice is about 40% and the evolution of the total area covered by melt ponds on multiyear ice is plotted in Figure 1 for comparison with observations [Nazintsev, 1964; Perovich et al., 2002b; Tschudi et al., 2001]. Table 1 summarizes some of the observations.

[36] The evolution of the mean melt pond area for first-year sea ice and multiyear sea ice is shown in Figure 5.

The mean area of melt ponds on multiyear sea ice after 5 days of melting was 17 m^2, as the ponds grew together this increased to 69 m^2 after 20 days, and by the end of the melt season (50 days), the mean pond area had decreased to 51 m^2 owing to vertical drainage and melt through. These results agree well with field observations showing a mean melt-pond size of 62 m^2 [Perovich and Tucker, 1997] even though both smaller mean pond sizes of 15 m^2 to 20 m^2 have been reported [Barber and Yackel, 1999] as well as larger mean melt pond sizes [Eicken, 1994]. Although the mean area of the first-year ice melt ponds is much greater than for multiyear ice, it can be seen from Figure 4b that this is largely caused by the presence of one very large melt pond. Melt ponds on smooth first-year ice are found to be interconnected [Fetterer and Untersteiner, 1998; Yackel et al., 2000] and are therefore larger than melt ponds on rougher ice.

[37] Figure 6 shows the evolution of the total area covered by melt ponds versus time using the multiyear ice topography for $s = 0.8$ cm/day, $m_i = 1.2$ cm/day, $m_p = 2$ cm/day and $\Pi_h = 3 \times 10^{-9}$ m^2. The density was varied between 800 kg/m^3 and 950 kg/m^3. When the density is low the ice is thinner and less area is covered by melt ponds since the water more easily drains through holes in the ice.

[38] Figure 7a shows the total ice surface ablation using the multiyear ice topography for $m_p = 1$ cm/day and a horizontal permeability of $\Pi_h = 3 \times 10^{-9}$ m^2 as the seepage rate is varied from $s = 0$ to 1.25 cm/day and the melt rate
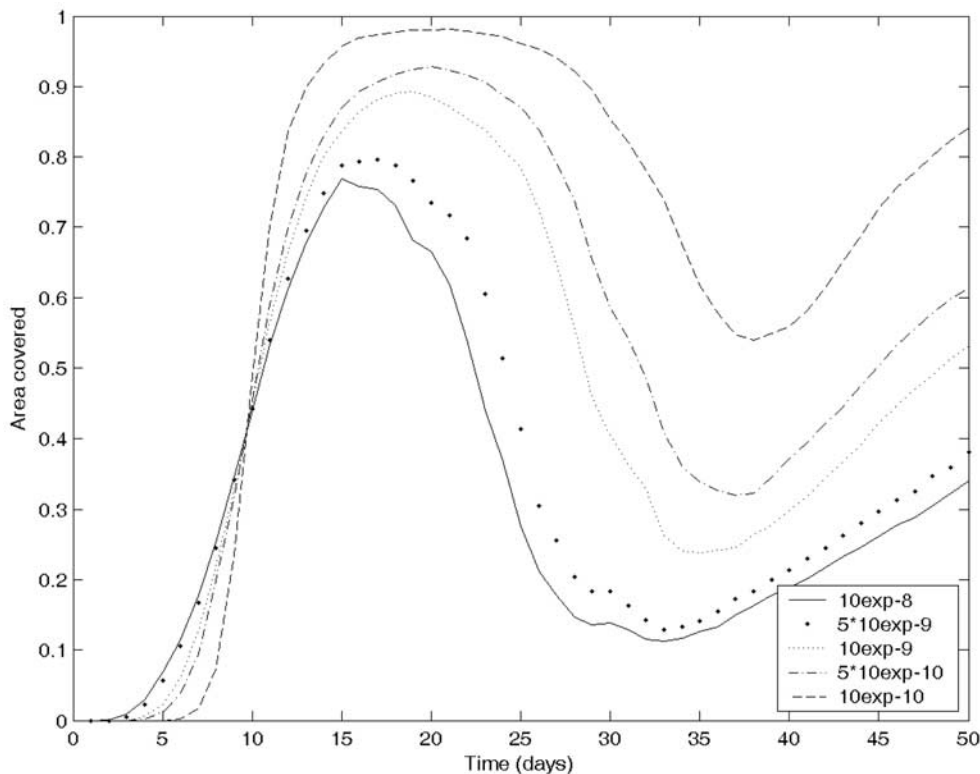
Figure 8b. Area covered by melt ponds on first-year sea ice for varying horizontal permeabilities Π_h. The legend shows the value of the horizontal permeability in m^2. The model used an initial first-year sea ice topography, seepage rate $s = 0.8$ cm/day, unponded ice melt rate $m_i = 1.2$ cm/day, and maximum melt pond enhanced melt rate $m_p = 2$ cm/day.

for unponded ice is varied from $m_i = 0.2$ to 1.45 cm/day. Figure 7b shows a similar plot except that $m_p = 2$ cm/day. From these plots we see that increasing the unponded ice melt rate m_i and the extra melt rate due to the presence of deep ponds m_p naturally increases the total surface ablation. Lowering the seepage rate s also increases the total surface ablation since a greater area will be covered by melt ponds and ponded ice melts more rapidly than unponded ice. When the seepage rate equals or exceeds the melt rate, no melt ponds are formed and the total surface ablation is determined simply by m_i and the melt season length.

[39] Figures 8a and 8b shows the melt pond area coverage versus time for multiyear sea ice and first-year sea ice, respectively, for five different values of the horizontal permeability, $\Pi_h = 10^{-8}$, 5×10^{-9}, 10^{-9}, 5×10^{-10}, and 10^{-10} m^2, for $s = 0.8$ cm/day, $m_i = 1.2$ cm/day, and $m_p = 2$ cm/day. When the permeability is low, surface meltwater is distributed horizontally relatively slowly so that melt ponds take longer to accumulate and are relatively shallow.

[40] Figure 9 shows the total surface ablation for first-year ice and multiyear sea ice versus the maximum enhanced melt rate beneath melt ponds m_p, for $s = 0.8$ cm/day, $m_i = 1.2$ cm/day, and $\Pi_h = 3 \times 10^{-9}$ m^2. For m_p less than about 2.5 cm/day, increasing m_p leads to an increase in the surface ablation for first-year ice whereas the surface ablation decreases for higher values of m_p. For multiyear ice the surface ablation increases with

higher values of m_p but the effect gets smaller for high values. For higher values of m_p the ponds tend to melt through completely, draining the surrounding area, and reducing the surface ablation rate.

[41] Figure 10 shows the maximum area covered by melt ponds on multiyear ice, and Figure 11a shows the total surface ablation, as the melt rate of unponded ice m_i was varied from 1 cm/day to 3.5 cm/day and m_p was varied from 0 cm/day to 3 cm/day. Figure 11b shows the total surface ablation for first-year ice. The other parameter values were $s = 0.8$ cm/day and $\Pi_h = 3 \times 10^{-9}$ m^2. The maximum area covered by melt ponds increases with the melt rate of unponded ice but decreases as the maximum extra melt rate beneath melt ponds m_p is increased, as this leads to fewer, deeper ponds. As one would expect, the total amount of surface ablation increases as either, or both of, m_i are m_p are increased.

5. Discussion of Results

[42] Topography has been found to be an important factor in determining the area covered in melt ponds. For the same model parameters but different initial surface topographies, i.e., those describing first-year sea ice and multiyear sea ice, the difference in the maximum area coverage of melt ponds exceeded 40% of the total area. The variation in maximum coverage of melt ponds within the multiyear ice and first-year ice topographies tested is around 20% of the total area. This conclusion broadly
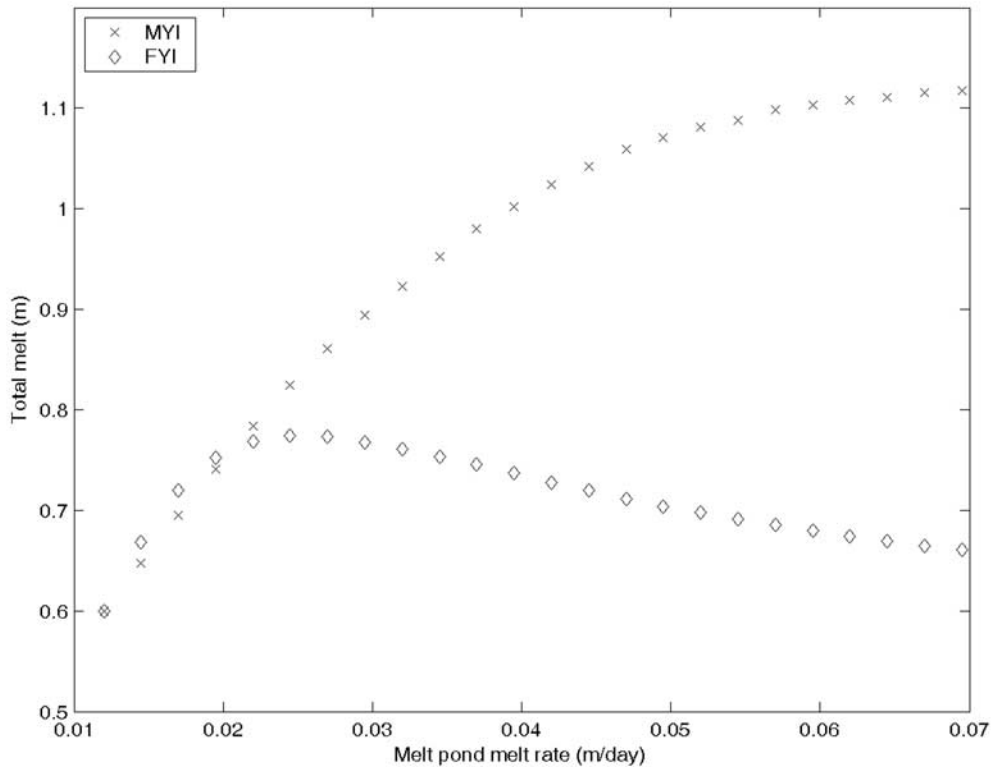
Figure 9. Total summer surface ablation of multiyear sea ice and first-year sea ice for varying melt rates beneath melt ponds. The model used a seepage rate $s = 0.8$ cm/day, a horizontal permeability $\Pi_h = 3 \times 10^{-9}$ m^2, and an unponded ice melt rate of $m_i = 1.2$ cm/day.

agrees with observations of pond fraction on multiyear and first-year sea ice obtained from National Technical Means Data described by *Fetterer and Untersteiner* [1998, Figure 11] and the field observations cited by *Eicken et al.* [2004, Figure 9]. The total surface ablation with the standard set of parameters of 0.92 m for multiyear sea ice is slightly higher than measured average surface ablations of multiyear sea ice of 0.3 m to 0.7 m reported by *Untersteiner* [1990] and *Golovin et al.* [1996]. Model simulations predict surface ablations of 0.40 m [*Maykut and Untersteiner*, 1971], 0.57 m [*Ebert and Curry*, 1993] and 0.92 m [*Taylor and Feltham*, 2004], although the latter simulation was for ponded ice only. Our modeled total surface ablation of first-year sea ice was 0.76 m (0.16 m less than the multiyear sea ice), but the first-year ice melted through almost completely.

[43] The relative importance of variation in our model parameters to the total surface ablation was determined by calculating the value of the sensitivity parameter

$$\delta_{sens}(x) = \frac{\langle x \rangle}{\langle A \rangle} \frac{\partial A}{\partial x}, \qquad (8)$$

where x is the model parameter, A is the total surface ablation, and the derivative is approximated in the vicinity of $s = 0.8$ cm/day, $m_i = 1.2$ cm/day, $m_p = 2$ cm/day, and $\Pi_h = 3 \times 10^{-9}$ m^2. The values $\langle x \rangle$ and $\langle A \rangle$ are the values of the parameter and the total surface ablation in the standard case, respectively, and their ratio serves to nondimensionalize the derivative. A positive value of the

sensitivity parameter implies that an increase in parameter x leads to an increase in the total surface ablation A and a negative value implies the reverse.

[44] In Table 2, we show the values of the sensitivity parameter for each of our model parameters s, m_i, m_p, and Π_h. We see that variation in vertical seepage s has a relatively large impact on total surface ablation. Decreasing the seepage rate for multiyear ice by 1 mm/day (to 0.7 cm/day) increased the total surface ablation by 0.03 m when the enhanced melt rate from the melt ponds was low ($m_p = 1$ cm/day) and by 0.06 m when the enhanced melt rate from the melt ponds was high ($m_p = 2$ cm/day). For first-year ice the increases were 0.03 m and 0.05 m for $m_p = 1$ cm/day and $m_p = 2$ cm/day, respectively. By contrast, it would appear that variation in the horizontal permeability Π_h seems to have relatively little impact on total surface ablation (provided that Π_h is greater than about 10^{-10} m^2). Changing the permeability for multiyear ice by a factor of 10 (from 10^{-8} m^2 to 10^{-9} m^2) increased the total surface ablation by 8%. We should, however, treat this result with considerable caution as the vertical seepage and horizontal flow are mutually dependent and a fuller model would explicitly calculate these flow rates.

[45] From Table 2, we see that the surface ablation rate of unponded ice is the most important parameter in determining the total surface ablation in the vicinity of the standard set of model parameters. Increasing the unponded melt rate m_i by 1 mm/day (to 1.3 cm/day) increases the total surface ablation by 0.07 m for $m_p =$
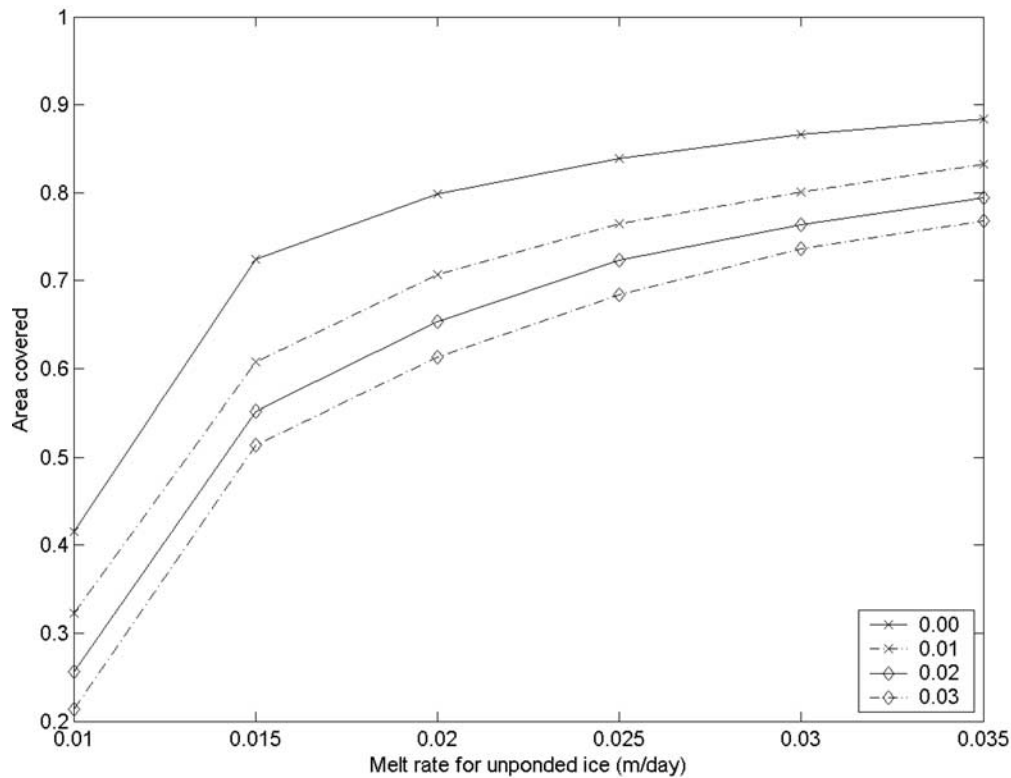
Figure 10. Maximum area covered by melt ponds on multiyear sea ice for different values of unponded sea ice melt rates m_i and maximum enhanced melt rate beneath melt ponds m_p. The legend shows the value of m_p in m/day. The model was initialized with a multiyear sea ice topography, a seepage rate of $s = 0.8$ cm/day, and a horizontal permeability $\Pi_h = 3 \times 10^{-9}$ m^2.

1 cm/day and by 0.10 m for $m_p = 2$ cm/day for multiyear ice. For first-year ice the increases were 0.05 m and 0.06 m for $m_p = 1$ cm/day and $m_p = 2$ cm/day, respectively. The maximum enhanced melt rate beneath the melt ponds m_p seems to be of relatively low importance in determining the total surface ablation. Increasing m_p leads to greater total melting for multiyear ice but, as the ponds form in depressions of typically shallow ice, the ponds melt through and drain the surrounding area. This tends to suppress the importance of the enhanced melt rate beneath ponds to the total surface ablation. Deep melt ponds which do not melt through, however, can have an important effect on the heat budget of the ice cover as they refreeze later, releasing latent heat.

6. Concluding Remarks

[46] A mathematical model was developed to help understand the relative importance of melting and drainage processes to the summer evolution of the sea-ice cover. Different topographies, unponded ice melt rates, melt rates beneath melt ponds, vertical drainage rates, and horizontal permeabilities were tested. Despite the simplicity of the model physics, the model is able to quantitatively capture the main features of melt-pond formation, spreading and drainage.

[47] Calculations using our model give new insight into processes important for melt pond development. In particular, topography, vertical seepage rate, and unponded ice melt rate turned out to be the most important unknowns in determining the total summer-time surface ablation of sea ice. However, the treatment of meltwater flow was relatively crude and the model does not explicitly treat a snow cover. The role of snow and the importance of hydrodynamic processes to determining melt pond evolution is described by *Eicken et al.* [2004, 2002]. On this basis of this, we can speculate about the typical role of snow in a model of melt pond evolution. In particular, as the snow cover melts before the ice beneath it, the distribution of snow will largely determine the initial source of meltwater at the beginning of the melt season. Since, at this time, the sea ice is relatively cold and therefore relatively impermeable, we would expect lateral spreading of melt ponds to dominate vertical drainage into the underlying ocean. This is especially true of flatter, first-year sea ice as the meltwater is not trapped in depressions. The lateral spread of melt ponds might be expected to lead to enhanced melt at this time (which is closer to the peak in solar radiation) leading to entire melt through of sea ice in places, draining meltwater from a surrounding catchment area. The net effect of this may well be to reduce total ablation as predicted by our existing model. To model these processes in a physically reasonable manner is the subject of ongoing research.

[48] First-year sea ice tends to be flatter and thinner than multiyear ice, and this had a significant impact on the
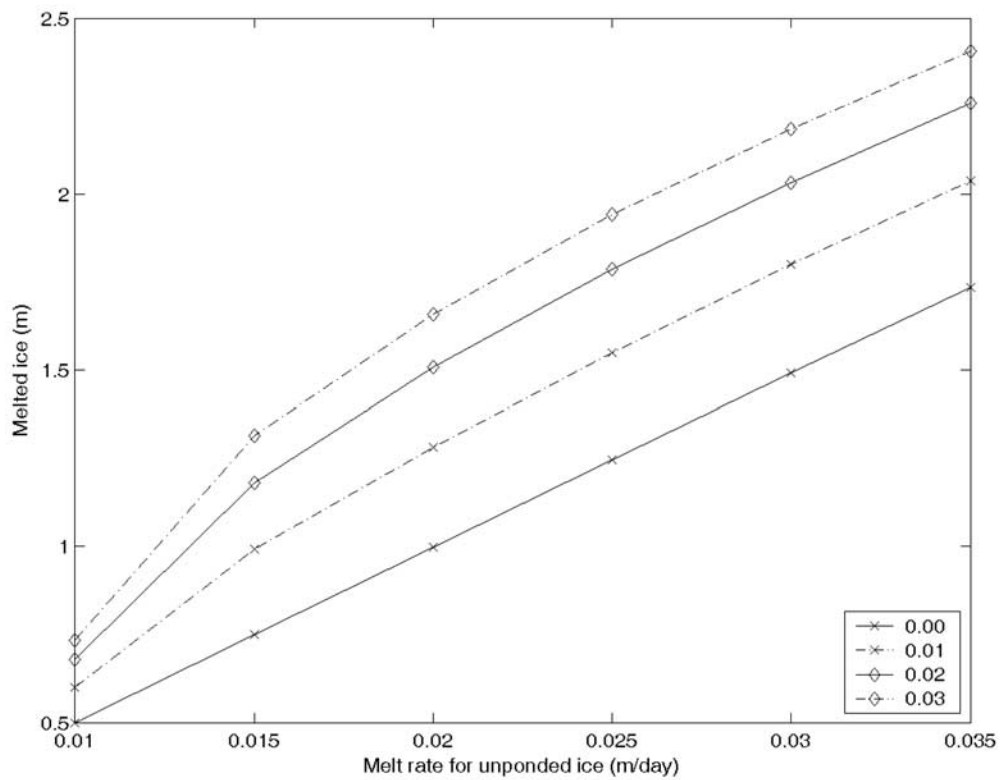
Figure 11a. Total amount of summer surface ablation for multiyear sea ice for different values of unponded sea ice melt rates m_i and maximum enhanced melt rate beneath melt ponds m_p. The legend shows the value of m_p in m/day. The model was initialized with a multiyear sea ice topography, a seepage rate of $s = 0.8$ cm/day, and a horizontal permeability $\Pi_h = 3 \times 10^{-9}$ m^2.
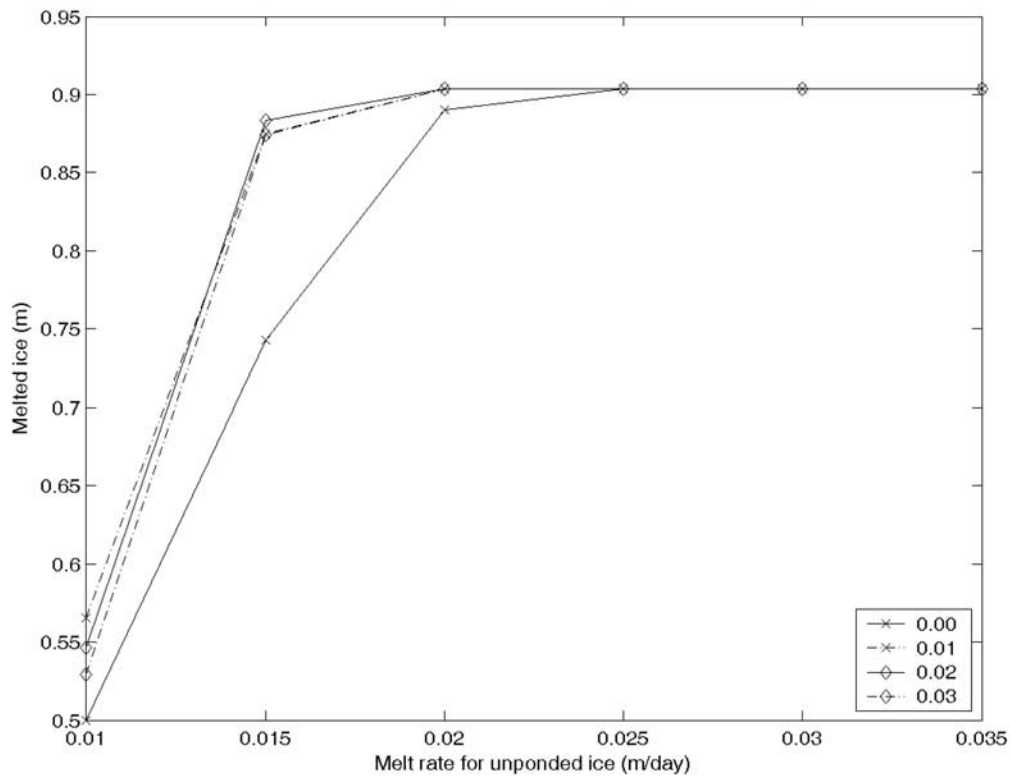
Figure 11b. Total amount of summer surface ablation for first-year sea ice for different values of unponded sea ice melt rates m_i and maximum enhanced melt rate beneath melt ponds m_p. The legend shows the value of m_p in m/day. The model was initialized with a first-year sea ice topography, a seepage rate of $s = 0.8$ cm/day, and a horizontal permeability $\Pi_h = 3 \times 10^{-9}$ m^2.

Table 2. Model's Sensitivity to Variation in Model Parameters[a]

Sensitivity	Ice Type	Seepage Rate s	Unponded Melt Rate m_i	Maximum Enhanced Melt Rate m_p	Horizontal Permeability Π_h
$\delta_{sens}(x)$	MYI	−0.53	1.30	0.26	−0.037
$\delta_{sens}(x)$	FYI	−0.64	1.22	−0.074	−0.046

[a]In the vicinity of $s = 0.8$ cm/day, $m_i = 1.2$ cm/day, $m_p = 2$ cm/day, and $\Pi_h = 3 \times 10^{-9}$ m^2.

simulations of surface melt. Fewer melt ponds were formed on first-year ice than multiyear ice, but these ponds were wider and less deep, covering up to 40% more of the floe's surface area. As noted in section 1, this conclusion is supported by remotely sensed observations and field measurements [*Derksen et al.*, 1997; *Eicken et al.*, 2004; *Fetterer and Untersteiner*, 1998; *Hanesiak et al.*, 2001; *Yackel et al.*, 2000 and references therein]. Interestingly, uncertainty in the enhanced melt rate of sea ice beneath melt ponds, due to the lower albedo of pond-covered ice, had a relatively small impact on total surface ablation. This was because ponds can melt through completely, draining the surrounding area. Given the large impact of uncertainty in model parameters and physics to the total summer-time surface ablation, and the expected increase in the relative abundance of first-year sea ice in the Arctic, we suggest that further study of summer melt processes is desirable.

References

Barber, D. G., and J. Yackel (1999), The physical, radiative and microwave scattering characteristics of melt ponds on Arctic landfast sea ice, *Int. J. Remote Sens.*, 20(10), 2069–2090.

Derksen, C. P., J. M. Piwowar, and E. F. LeDrew (1996), The quantification of sea ice melt features from low level aerial photographs, paper presented at *1996 International Geoscience and Remote Sensing Symposium (IGARSS'96)*, Inst. of Electr. and Electron. Eng., Waterloo, Ont., Canada.

Derksen, C., J. Piwowar, and E. LeDrew (1997), Sea-ice melt-pond fraction as determined from low level aerial photographs, *Arct. Alp. Res.*, 29(3), 345–351.

Ebert, E. E., and J. A. Curry (1993), An intermediate one-dimensional thermodynamic sea ice model for investigating ice-atmosphere interactions, *J. Geophys. Res.*, 98(C6), 10,085–10,109.

Ebert, E., J. L. Schramm, and J. A. Curry (1995), Disposition of solar radiation in sea ice and the upper ocean, *J. Geophys. Res.*, 100(C8), 15,965–15,975.

Eicken, H. (1994), Structure of under-ice melt ponds in the central Arctic and their effect on the sea-ice cover, *Limnol. Oceanogr.*, 39(3), 682–694.

Eicken, H., W. B. Tucker III, and D. K. Perovich (2001), Indirect measurements of the mass balance of summer Arctic sea ice with an electromagnetic induction technique, *Ann. Glaciol.*, 33, 194–200.

Eicken, H., H. R. Krouse, D. Kadko, and D. K. Perovich (2002), Tracer studies of pathways and rates of meltwater transport through Arctic summer sea ice, *J. Geophys. Res.*, 107(C10), 8046, doi:10.1029/2000JC000583.

Eicken, H., T. C. Grenfell, D. K. Perovich, J. A. Richter-Menge, and K. Frey (2004), Hydraulic controls of summer Arctic pack ice albedo, *J. Geophys. Res.*, 109, C08007, doi:10.1029/2003JC001989.

El Naggar, S., C. Garrity, and R. O. Ramseier (1998), The modelling of sea ice melt-water ponds for the high Arctic using an airborne line scan camera, and applied to the Satellite Special Sensor Microwave/Imager (SSM/I), *Int. J. Remote Sens.*, 19(12), 2373–2394.

Feltham, D. L., M. G. Worster, and J. S. Wettlaufer (2002), The influence of ocean flow on newly forming sea ice, *J. Geophys. Res.*, 107(C2), 3009, doi:10.1029/2000JC000559.

Fetterer, F., and N. Untersteiner (1998), Observations of melt ponds on Arctic sea ice, *J. Geophys. Res.*, 103(C11), 24,821–24,835.

Freitag, J. (1999), The hydraulic properties of Arctic sea ice—Implications for the small-scale particle transport (in German), *Ber. Polarforsch.* 325, 150 pp.

Golovin, P. N., S. V. Kochetov, and L. A. Timokhov (1996), Freshening of the underice layer due to melting, *Oceanology*, 35, 482–487.

Grenfell, T. C., and G. A. Maykut (1977), The optical properties of ice and snow in the Arctic basin, *J. Glaciol.*, 18(80), 445–463.

Grenfell, T. C., and D. K. Perovich (1984), Spectral albedos of sea ice and incident solar irradiance in the southern Beaufort Sea, *J. Geophys. Res.*, 89(C3), 3573–3580.

Hanesiak, J. M., D. G. Barber, R. A. De Abreu, and J. J. Yackel (2001), Local and regional albedo observations of arctic first-year sea ice during melt ponding, *J. Geophys. Res.*, 106(C1), 1005–1016.

Holt, B., and S. A. Digby (1985), Processes and imagery of first-year fast sea ice during the melt season, *J. Geophys. Res.*, 90(C3), 5045–5062.

Hvidegaard, S. M., and R. Forsberg (2002), Sea-ice thickness from airborne laser altimetry over the Arctic Ocean north of Greenland, *Geophys. Res. Lett.*, 29(20), 1952, doi:10.1029/2001GL014474.

Kundu, P. K. (1990), *Fluid Mechanics*, Elsevier, New York.

Langleben, M. (1968), Albedo measurements of an Arctic ice cover from high towers, *J. Glaciol.*, 7(50), 289–297.

Laxon, S., N. Peacock, and D. Smith (2003), High interannual variability of sea ice thickness in the Arctic region, *Nature*, 425, 947–950.

Makshtas, A. P., and I. A. Podgorny (1996), Calculation of melt pond albedos on Arctic sea ice, *Polar Res.*, 15(1), 43–52.

Maykut, G. A., and N. Untersteiner (1971), Some results from a time-dependent thermodynamic model of sea ice, *J. Geophys. Res.*, 76(6), 1550–1575.

McPhee, M. G., T. P. Stanton, J. H. Morison, and D. G. Martinson (1998), Freshening of the upper ocean in the Central Arctic: Is perennial sea ice disappearing?, *Geophys. Res. Lett.*, 25(10), 1729–1732.

Morassutti, M. P. (1992), Component reflectance scheme for DMSP-derived sea ice reflectances in the Arctic Basin, *Int. J. Remote Sens.*, 13(4), 647–662.

Morassutti, M. (1995), Sea ice melt pond data from the Canadian Arctic, Natl. Snow and Ice Data Cent., Boulder, Colo. (Available at http://nsidc.org/data/docs/noaa/g01169_seaice_melt_pond/index.html)

Morassutti, M. P., and E. F. LeDrew (1996), Albedo and depth of melt ponds on sea-ice, *Int. J. Climatol.*, 16, 817–838.

Nazintsev, Y. L. (1964), Thermal balance of the surface of the perennial ice cover in the central Arctic (in Russian), *Tr. Ark. Antark. Nauchno Issled. Inst.*, 267, 110–126.

Notz, D., M. G. McPhee, M. G. Worster, G. A. Maykut, K. H. Schlünzen, and H. Eicken (2003), Impact of underwater-ice evolution on Arctic summer sea ice, *J. Geophys. Res.*, 108(C7), 3223, doi:10.1029/2001JC001173.

Papakyriakou, T. N. (1999), An examination of relationships among the energy balance, surface properties and climate over snow covered sea ice during the spring season, Ph.D. thesis, Univ. of Waterloo, Waterloo, Ont., Canada.

Perovich, D. K., and W. B. Tucker III (1997), Arctic sea-ice conditions and the distribution of solar radiation during summer, *Ann. Glaciol.*, 25, 445–450.

Perovich, D. K., T. C. Grenfell, B. Light. J. A. Richter-Menge, M. Sturm, W. B. Tucker III, H. Eicken, G. A. Maykut, and B. Elder (1999), *SHEBA: Snow and Ice Studies, Version 1.0* [CD-ROM], Cold Regions Res. and Eng. Lab., Hanover, N. H.

Perovich, D. K., T. C. Grenfell, B. Light, and P. V. Hobbs (2002a), Seasonal evolution of the albedo of multiyear Arctic sea ice, *J. Geophys. Res.*, 107(C10), 8044, doi:10.1029/2000JC000438.

Perovich, D. K., W. B. Tucker III, and K. A. Ligett (2002b), Aerial observations of the evolution of ice surface conditions during summer, *J. Geophys. Res.*, 107(C10), 8048, doi:10.1029/2000JC000449.

Perovich, D. K., T. C. Grenfell, J. A. Richter-Menge, B. Light, W. B. Tucker III, and H. Eicken (2003), Thin and thinner: Sea ice mass balance measurements during SHEBA, *J. Geophys. Res.*, 108(C3), 8050, doi:10.1029/2001JC001079.

Smith, D. M. (1998), Recent increase in the length of the melt season of perennial Arctic sea ice, *Geophys. Res. Lett.*, 25(5), 655–658.

Taylor, P. D., and D. L. Feltham (2004), A model of melt pond evolution on sea ice, *J. Geophys. Res.*, 109, C12007, doi:10.1029/2004JC002361.

Tschudi, M. A., J. A. Curry, and J. A. Maslanik (2001), Airborne observations of summertime surface features and their effect on surface albedo during FIRE/SHEBA, *J. Geophys. Res.*, 106(D14), 15,335–15,344.

Untersteiner, N. (1961), On the mass and heat budget of Arctic sea ice, *Arch. Meteorol. Geophys. Bioklimatol., Ser. A*, 12, 151–182.

Untersteiner, N. (1990), Structure and dynamics of the Arctic Ocean ice cover, in *The Arctic Ocean Region*, edited by A. Grantz, L. Johnson, and J. F. Sweeney, pp. 37–51, Geol. Soc. of Am., Boulder, Colo.

Yackel, J. J., D. G. Barber, and J. M. Hanesiak (2000), Melt ponds on sea ice in the Canadian Archipelago: 1. Variability in morphological and radiative properties, *J. Geophys. Res.*, 105(C9), 22,049–22,060.

————————

D. L. Feltham and P. D. Taylor, Centre for Polar Observation and Modeling, Department of Space and Climate Physics, University College London, Pearson Building, Gower Street, London WC1E 6BT, UK. (dlf@cpom.ucl.ac.uk; pdt@cpom.ucl.ac.uk)

M. Lüthje, Ørsted-DTU, Ørsted Plads, Building 348, DK-2800 Kgs. Lyngby, Denmark. (mikael@lythje.com)

M. G. Worster, Institute of Theoretical Geophysics, Department of Applied Mathematics and Theoretical Physics, University of Cambridge, CMS, Wilberforce Road, Cambridge CB30WA, UK. (grae@esc.cam.ac.uk)